Mimicking a negative refractive slab by combining two phase conjugators

Alexandre Aubry* and J. B. Pendry

The Blackett Laboratory, Imperial College, Prince Consort Road, London SW7 2BZ, UK
**Corresponding author: a.aubry@imperial.ac.uk*

Received September 11, 2009; revised November 3, 2009; accepted November 6, 2009;
posted November 9, 2009 (Doc. ID 117080); published December 18, 2009

A new route toward a lossless superlens has been proposed recently. It relies on the association of two phase-conjugating sheets. The aim of this study is to show how such a lens can be implemented experimentally at optical frequencies. Because efficient phase conjugation of evanescent waves is illusory with the current technology, only the case of propagating waves is considered here. Four wave mixing in $BaTiO_3$ is shown to provide efficient backward and forward phase conjugation over a major part of the angular spectrum, taking advantage of internal reflections inside the non-linear slab. However, phase distortions arise for high spatial frequencies and limit the resolving power of the device. The addition of a second phase-conjugator automatically compensates for these phase distortions. The wave field is then perfectly translated through the system. Actually, such a device performs even better than a negative refracting lens since the association of two phase-conjugating mirrors behaves like a resonant cavity. An amplification of the wave field by a factor of 10^2 in intensity is predicted, despite the important absorption in $BaTiO_3$. © 2009 Optical Society of America

OCIS codes: 190.5040, 190.4380, 110.2990.

1. INTRODUCTION

Since the seminal work of Pendry [1], the concept of a perfect lens has attracted considerable attention (see, e.g., [2–4] and references therein). A flat slab made of a negative refractive metamaterial ($\epsilon=\mu=-1$), usually referred to as a Veselago's lens [5], is shown to not only focus the propagating wave field, but also the evanescent components of radiation that generally remains confined in the near-field. Therefore, Veselago's lens may overcome the classical limit of diffraction and sub-wavelength imaging may be performed. Experimental works have confirmed these theoretical predictions, first in the microwave regime [6] and then at optical frequencies [7]. However, the major limitation of Veselago's lens comes from absorption which drastically reduces the resolving power of the superlens [2,8–10].

To overcome the absorption issue, a new route toward a lossless superlens scheme has been proposed in a recent paper [11]. The key idea is to benefit from the link that exists between phase conjugation (PC) and negative refraction [12,13]. A PC mirror has the property to reverse both the propagation direction and the phase of an incident wave field. A backward phase-conjugated wave is then produced. Now, let us imagine a phase-conjugating sheet (PCs) performing forward PC. In that case, only the transverse component of the wave vector is reversed and an obvious link with the negative refractive interface is found. The analogy can be carried on by considering a superlens based on the combination of two PCs's performing both backward and forward PC [11]. Similarly to a negative refractive slab, the propagating wave field is shown to be perfectly translated through the system by a distance $2d$ (d being the distance between the two PCs's; see Fig. 1). Moreover, if the reflectivity R of each PCs is sufficiently large to compensate for the exponential decay of evanescent waves, the device may also be able to image the near fields, taking advantage of the multiple scattering process between the two PCs's. Hence, sub-wavelength imaging is possible and, in the limit $R\rightarrow\infty$, the image tends to perfection.

Unlike the superlens based on negative refraction [1], loss is no longer an issue here since the wave field propagates through vacuum. However, the crucial point is to find a highly non-linear surface capable of phase conjugating efficiently the evanescent wave field. Unfortunately, this seems illusory at optical frequencies with the current technology. Some experiments have pointed out the PC of optical near-fields, but it only concerns waves that are evanescent in air but propagative in the non-linear medium [14–16]. Consequently, we will restrict our study to the propagating wave field. Although sub-wavelength imaging is not reachable in this case, the combination of two PCs's keeps significant interest. First, such a device is an *absolute* optical instrument [17,18]: it reproduces stigmatically a three-dimensional (3D) domain and the optical length of any curve in the object space is equal to the optical length of its image. This system is thus capable of 3D imaging. Figure 1 illustrates this fact by comparing the axial imaging properties obtained with our system and the combination of two convergent lenses. Whereas the wave field is perfectly translated through the two PCs's, the association of two convergent lenses leads to both lateral and axial distortions of the image. Furthermore, we will show that a device consisting of two PCs's behaves like a resonant cavity. This may lead to a significant amplification of the imaged wave field.

The first axis of this work is to show how a forward

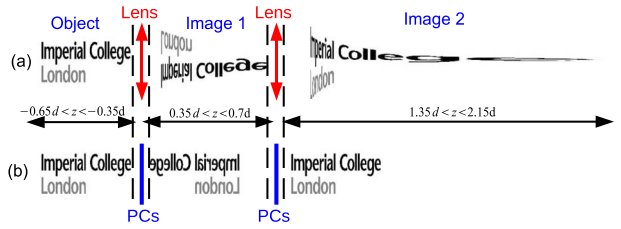

Fig. 1. (Color online) Imaging properties of a device combining (a) two convergent lenses and (b) two PCs's placed at $z=0$ and $z=d$, assuming geometrical optics. The focal length of the lenses is $d/4$.

phase-conjugator dedicated to imaging purposes can be implemented experimentally at optical frequencies. As suggested in [11], the best candidate for the PC is degenerate four-wave mixing (FWM) technique [19–22]. FWM is closely analogous to real-time holography in which a pump wave $\mathbf{E_1}$ is used to record a hologram of an object wave $\mathbf{E_3}$ (see Fig. 2). The hologram is then subsequently read with a second pump wave $\mathbf{E_2}$ which propagates in an opposite direction to $\mathbf{E_1}$. A phase-conjugated wave $\mathbf{E_4}$ is then created. The non-linear media that can be used to perform degenerate FWM are Kerr-like [23–26], resonant (absorbing or amplifying) [27–33], or photorefractive (PR) media [34–39]. In our study, FWM in PR crystals will be considered since the PR effect may provide an efficient and uniform PC process over a major part of the angular spectrum, under certain conditions. This is a promising perspective for imaging purposes since an optical device requires an aperture angle as large as possible. The PR medium we consider in this study is barium titanate ($BaTiO_3$) which is known for its strong electro-optic properties. The c-axis is chosen to be oriented perpendicular to the PR slab interface.

Classical FWM (i.e., with two counter-propagating pump beams) only allows backward PC. In the literature, a special FWM arrangement has been proposed to perform forward PC [40]. The two pump beams are no longer counter-propagating but come from the same side of the non-linear slab. The idea is then to adjust the angle of intersection between the two pump beams as a function of the angle of incidence of the probe wave $\mathbf{E_3}$. This arrangement is only valid over a very restricted angular domain

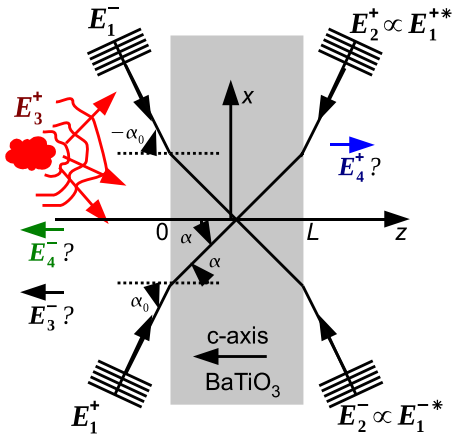

Fig. 2. (Color online) Experimental configuration considered for FWM.

(typically a few milliradians) and hence does not apply to arbitrary wave-fronts. The same argument holds for forward three wave mixing in a second-order non-linear medium [41,42]. Indeed, a simpler idea is to directly take advantage of the internal reflections inside the non-linear slab to perform simultaneously forward and backward PC over the whole angular spectrum. Albeit simpler and more powerful, this way of performing forward PC has only been investigated in a few studies, both theoretically [43] and experimentally [44,45].

The first originality of our work lies in the theoretical treatment of forward PC and its application to imaging. It consists in first determining the experimental conditions needed to have an efficient and uniform PC process both in reflection and transmission over a major part of the angular spectrum. Contrary to previous work [43], the coupling coefficient, which is the key parameter of PC, is not assumed constant but its expression is derived theoretically as a function of all the physical parameters that play a role in the PR effect. In particular, the coupling coefficient is shown to be opposite for backward and forward PC in our experimental configuration. This fact is crucial since it may act drastically and positively on the efficiency of the forward PC process. Once the coupling coefficient is known, the transmission and reflection coefficients for the PC process are derived analytically. A phenomenon of double forward PC is predicted: due to the wave reflections on each interface of the PR slab, the forward phase-conjugated wave contains two contributions, each one focusing at different depths. Note that this phenomenon has already been pointed out experimentally [44] but, to our knowledge, not investigated theoretically. Double forward PC is clearly an issue for 3D imaging but can be circumvented by adding an anti-reflective coating on the first interface of the PR slab. Phase distortions undergone by the high frequency components of the forward phase-conjugated wave-front are also predicted. They are due to the difference of refractive index between air and the PR medium. These phase distortions lead to a displacement of the focal spot and limit the angular aperture of the forward phase-conjugator. At last, our theoretical study takes into account the absorption losses. Analytical expressions of the transmission and reflection coefficients are derived in the presence of absorption and allow one to study its influence on the PC process.

The second axis of this work deals with the connection between PC and negative refraction. First we show that the addition of a second PCs automatically compensates the phase distortions undergone by the forward phase-conjugated wave-front at the first PCs. The propagating wave field is thus perfectly translated through the device, hence mimicking a negative refractive lens. Actually it performs even better than negative refraction since the two phase-conjugating mirrors behave like a resonant cavity. Consequently, the wave field is amplified through the device. In theory, this amplification could be infinite since the PC reflectivity is close to unity in PR media. However, absorption losses limit this amplification process in practice. The influence of absorption is investigated theoretically and an amplification by a factor of 10^2 in intensity is predicted despite the important absorption in $BaTiO_3$.

Table 1. Physical Properties of $BaTiO_3$ and Experimental Conditions

Index of refraction (o) [46]	$n_o = 2.437$
Index of refraction (e) [46]	$n_e = 2.365$
Dielectric constant (F/m) [46]	$\epsilon_{\parallel} = 106\epsilon_0$, $\epsilon_{\perp} = 4300\epsilon_0$
Acceptor density (m^{-3}) [47]	$N_A = 2 \times 10^{22}$
Electro-optic coefficients (m/V) (unclamped values [48,49])	$r_{13} = 25 \times 10^{-12}$, $r_{33} = 50 \times 10^{-12}$, $r_{42} = 1300 \times 10^{-12}$
Linear absorption (m^{-1}) [50]	$a = 150$
Wavelength (m)	$\lambda = 514.5 \times 10^{-9}$ (Ar^+ laser)
Temperature (K)	$T = 290$

2. FORWARD PC PROVIDED BY INTERNAL REFLECTIONS

In this section, the PC process taking place in a slab of $BaTiO_3$ is investigated taking into account internal reflections. The transmission and reflection coefficients for the PC process are derived and allow one to determine the experimental conditions needed to obtain a uniform and efficient PC process for each angular component of the wave field. Undesirable effects like double forward PC and phase distortions are pointed out and their consequences on imaging are discussed.

A. Experimental Configuration

The basic interaction geometry is shown in Fig. 2. Let us consider a slab of $BaTiO_3$ extending indefinitely in the x and y directions, and from $z = 0$ to L in the z direction. The physical properties of $BaTiO_3$, as well as the experimental conditions we consider, are summarized in Table 1. The crystal axis is chosen to be aligned in the opposite direction to the z-axis. Note that this choice is not arbitrary: we will see that this configuration allows an efficient PC process over a major part of the angular spectrum, both in reflection and transmission. To observe the largest electro-optic effects in $BaTiO_3$, it is necessary to use extraordinary polarizations. To that aim, each interacting beam is assumed to be p-polarized.

The PR slab is pumped by two couples of counter-propagating plane waves $\mathbf{E_1^{\pm}}$ and $\mathbf{E_2^{\pm}}$ of frequency ω. Introducing two couples of counter-propagating pump beams is not necessary experimentally since one is sufficient for FWM. However, this simplifies the problem theoretically, making it symmetric, and improves the efficiency of the PC process. Note that this second couple of pump beams appears anyway in practice due to the internal reflections in the PR slab. These pumps are assumed to be undepleted and to remain plane waves in the non-linear medium. Inside the slab, the electric fields of the pump beams can be expressed as

$$\mathbf{E_1^{\pm}}(\mathbf{r},t) = A_1 \hat{\mathbf{e}}_{\pm\alpha} e^{-i(\omega t - \mathbf{q}^{\pm}\cdot\mathbf{r})} + \text{c.c.}, \quad (1)$$

$$\mathbf{E_2^{\pm}}(\mathbf{r},t) = A_2 \hat{\mathbf{e}}_{\pm\alpha} e^{-i(\omega t + \mathbf{q}^{\pm}\cdot\mathbf{r})} + \text{c.c.}, \quad (2)$$

with

$$\hat{\mathbf{e}}_{\pm\alpha} = \cos\,\alpha\,\mathbf{u_x} \mp \sin\,\alpha\,\mathbf{u_z},$$

$$\mathbf{q}^{\pm} = \pm \sin\,\alpha\,\mathbf{u_x} + \cos\,\alpha\,\mathbf{u_z},$$

where c.c. stands for complex conjugate. $\pm\alpha$ denotes the angle of refraction of the pump beams. $\mathbf{q}^{\pm}$ represents the wave vector of $\mathbf{E_1^{\pm}}$. The unitary vector $\hat{\mathbf{e}}_{\pm\alpha}$ designs the polarization direction of the pump wave fields. $\mathbf{u_x}$ and $\mathbf{u_z}$ are unitary vectors along the x and z directions. We solve the problem in steady state so that the amplitudes A_j are taken to be time independent. For the sake of simplicity, we assume that the beams $\mathbf{E_1^+}$ and $\mathbf{E_1^-}$ are of same amplitude A_1. Furthermore, we will assume that the amplitudes of the counter-propagating pump beams are opposite such that $A_2 = -A_1$. This is experimentally the case if the beams $\mathbf{E_2^{\pm}}$ are obtained by reflection of $\mathbf{E_1^{\pm}}$ on a silvered mirror.

Our aim is to study the PC process undergone by an arbitrary wave-front $\mathbf{E_3^+}$ (see Fig. 2). The physical process that occurs in the presence of internal reflections is illustrated in Fig. 3 and can be described as follows. A part of the probe wave $\mathbf{E_3^+}$ is transmitted through the interface $z = 0$. It interacts with counter-propagating pump beams through the PR effect, which gives rise to a backward phase-conjugated wave $\mathbf{E_4^-}$. $\mathbf{E_3^+}$ can also be reflected by the second interface at $z = L$, which results in a backward probe wave $\mathbf{E_3^-}$. The forward phase-conjugated wave $\mathbf{E_4^+}$ can then be generated either by the reflection of $\mathbf{E_4^-}$ on the interface $z = 0$ or by PC of $\mathbf{E_3^-}$. Consequently, our problem consists of four partial waves which are linked to each other either by a PC process ($\mathbf{E_3^+} \Leftrightarrow \mathbf{E_4^-}$, $\mathbf{E_4^+} \Leftrightarrow \mathbf{E_3^-}$) or by internal reflections ($\mathbf{E_3^+} \Leftrightarrow \mathbf{E_3^-}$, $\mathbf{E_4^-} \Leftrightarrow \mathbf{E_4^+}$). These four fields can be expressed as

$$\mathbf{E_3^{\pm}}(\mathbf{r},t) = \mathbf{A_3^{\pm}}(\mathbf{r}) e^{-i\omega t} + \text{c.c.}, \quad (3)$$

$$\mathbf{E_4^{\pm}}(\mathbf{r},t) = \mathbf{A_4^{\pm}}(\mathbf{r}) e^{-i\omega t} + \text{c.c.} \quad (4)$$

Let us decompose the probe and conjugated wave amplitudes into their plane wave components (see Fig. 4),

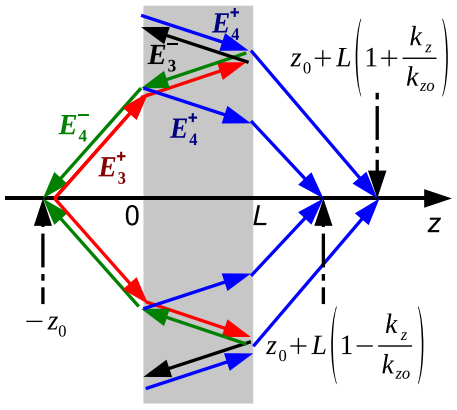

Fig. 3. (Color online) Scheme describing the paths taken by the four partial waves propagating inside the non-linear slab. E_4^+ can be produced either by reflection of E_4^- or by PC of E_3^-. It results in two images located at $z = z_o + L(1 \pm n^{-1})$.

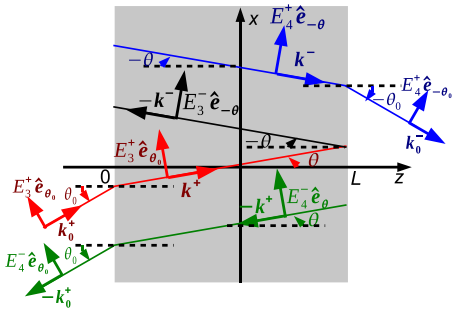

Fig. 4. (Color online) Notations and conventions used to describe the four partial waves propagating inside the non-linear slab. $\mathbf{k_0^{\pm}}=k_{z_0}\mathbf{u_z}\pm k_{\|}\mathbf{u_x}$ and $\mathbf{k^{\pm}}=k_z\mathbf{u_z}\pm k_{\|}\mathbf{u_x}$.

$$\mathbf{A_3^{\pm}}(\mathbf{r})=\begin{cases}\int A_3^{\pm}(k_{\|},z)\hat{\mathbf{e}}_{\pm\theta_0}e^{ik_{\|}\mathbf{r}_{\|}}e^{\pm ik_{zo}z}\mathrm{d}k_{\|} & \text{if } \mathbf{r}\notin\Omega\\ \int A_3^{\pm}(k_{\|},z)\hat{\mathbf{e}}_{\pm\theta}e^{ik_{\|}\mathbf{r}_{\|}}e^{\pm ik_{z}z}\mathrm{d}k_{\|} & \text{if } \mathbf{r}\in\Omega,\end{cases} \tag{5}$$

$$\mathbf{A_4^{\pm}}(\mathbf{r})=\begin{cases}\int A_4^{\pm}(-k_{\|},z)\hat{\mathbf{e}}_{\mp\theta_0}e^{-ik_{\|}\mathbf{r}_{\|}}e^{\mp ik_{zo}z}\mathrm{d}k_{\|}, & \text{if } \mathbf{r}\notin\Omega\\ \int A_4^{\pm}(-k_{\|},z)\hat{\mathbf{e}}_{\mp\theta}e^{-ik_{\|}\mathbf{r}_{\|}}e^{\mp ik_{z}z}\mathrm{d}k_{\|}, & \text{if } \mathbf{r}\in\Omega,\end{cases} \tag{6}$$

with

$$k_{zo}=\sqrt{\frac{\omega^2}{c_0^2}-k_{\|}^2},\quad k_z=\sqrt{n^2\frac{\omega^2}{c_0^2}-k_{\|}^2},$$

$$\theta_0=\arctan\left[\frac{k_{\|}}{k_{zo}}\right],\quad \theta=\arctan\left[\frac{k_{\|}}{k_z}\right].$$

Ω represents the spatial domain occupied by the PR slab. $k_{\|}$ is the transverse component of the wave vector. k_{zo} and k_z are the longitudinal components of the wave vector outside and inside the PR slab, respectively. n is the refractive index of the PR medium. θ_0 and θ are the angles of incidence and refraction. The unitary vectors $\hat{\mathbf{e}}_{\pm\theta_0}$ and $\hat{\mathbf{e}}_{\pm\theta}$ design the polarization directions of each plane wave component (see Fig. 4). Thanks to this linear decomposition, one can solve the problem considering each plane wave component separately.

B. Coupled Wave Equations

As shown in the literature [38,46], the PC process that occurs between $\mathbf{E_3^+}$ and $\mathbf{E_4^-}$ can be modeled by the following two coupled wave equations:

$$\frac{\mathrm{d}A_3^{+*}}{\mathrm{d}z}-\frac{\gamma(\theta)}{2}A_3^{+*}+\frac{a'}{2}A_3^{+*}=-\frac{\gamma(\theta)}{2}A_4^{-}, \tag{7}$$

$$\frac{\mathrm{d}A_4^{-}}{\mathrm{d}z}-\frac{\gamma(\theta)}{2}A_4^{-}-\frac{a'}{2}A_4^{-}=-\frac{\gamma(\theta)}{2}A_3^{+*}, \tag{8}$$

where $a'=a/\cos\theta$, with a being the linear absorption in the crystal. γ is the coupling coefficient which represents the strength of the non-linear process. Its expression is derived in our experimental configuration in the Appendix. Besides being a function of the angles of incidence of pump and probe waves, γ depends on the numerous physical parameters that play a role in the PR effect (electro-optic coefficients, dielectric constants, acceptor density, temperature, wavelength, etc.) [38]. γ has been computed considering the experimental conditions summarized in Table 1. Its evolution as a function of θ_0 and α_0 is shown in Fig. 5.

The same kind of coupled equations can be derived for the PC process between $\mathbf{E_3^-}$ and $\mathbf{E_4^+}$,

$$\frac{\mathrm{d}A_3^{-*}}{\mathrm{d}z}+\frac{\gamma'(-\theta)}{2}A_3^{-*}-\frac{a'}{2}A_3^{-*}=\frac{\gamma'(-\theta)}{2}A_4^{+}, \tag{9}$$

$$\frac{\mathrm{d}A_4^{+}}{\mathrm{d}z}+\frac{\gamma'(-\theta)}{2}A_4^{+}+\frac{a'}{2}A_4^{+}=\frac{\gamma'(-\theta)}{2}A_3^{-*}, \tag{10}$$

where γ' is the coupling coefficient associated with the PC process between $\mathbf{E_3^-}$ and $\mathbf{E_4^+}$. Due to the orientation of the c-axis, one can show that

$$\gamma'(-\theta)=-\gamma(\theta). \tag{11}$$

Finally Eqs. (9) and (10) become similar to Eqs. (7) and (8),

$$\frac{\mathrm{d}A_3^{-*}}{\mathrm{d}z}-\frac{\gamma(\theta)}{2}A_3^{-*}-\frac{a'}{2}A_3^{-*}=-\frac{\gamma(\theta)}{2}A_4^{+}, \tag{12}$$

$$\frac{\mathrm{d}A_4^{+}}{\mathrm{d}z}-\frac{\gamma(\theta)}{2}A_4^{+}+\frac{a'}{2}A_4^{+}=-\frac{\gamma(\theta)}{2}A_3^{-*}. \tag{13}$$

The two systems of coupled equations [Eqs. (7) and (8) and Eqs. (12) and (13)] lead to the same steady state equation for A_4^+ and A_4^-,

$$\frac{\mathrm{d}^2A_4^{\pm}}{\mathrm{d}z^2}-\gamma\frac{\mathrm{d}A_4^{\pm}}{\mathrm{d}z}-\frac{a'^2}{4}A_4^{\pm}=0. \tag{14}$$

We now assume that the absolute value of the coupling coefficient γ is superior to the absorption term a': $|\gamma|>a'>0$. In the contrary case, absorption losses would cancel out the forward PC process. Under this assumption, the forward and backward phase-conjugated amplitudes can be expressed as

$$A_4^{+}(-k_{\|},z)=e^{\gamma z/2}[Ce^{\eta\gamma z/2}+De^{-\eta\gamma z/2}], \tag{15}$$

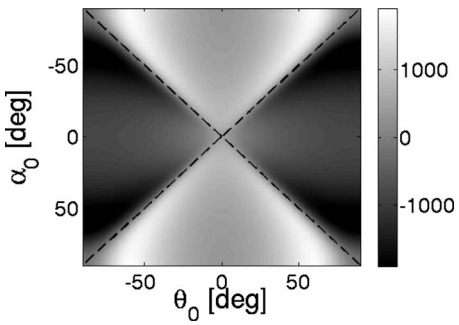

Fig. 5. Evolution of the coupling coefficient γ (m^{-1}) as a function of θ_0 and α_0 considering the physical properties of $BaTiO_3$ and experimental conditions given in Table 1.

$$A_4^-(-k_\parallel,z) = e^{\gamma z/2}[Ee^{\eta\gamma z/2} + Fe^{-\eta\gamma z/2}], \tag{16}$$

where $\eta = \sqrt{1-a'^2/\gamma^2}$. C, D, E, and F are constants which, so far, are arbitrary. Using Eqs. (8) and (13), the expressions of A_3^- and A_3^+ are deduced,

$$A_3^{-*}(k_\parallel,z) = -e^{\gamma z/2}[C(\eta + \sqrt{1-\eta^2})e^{\eta\gamma z/2} + D(-\eta + \sqrt{1-\eta^2})e^{-\eta\gamma z/2}], \tag{17}$$

$$A_3^{+*}(k_\parallel,z) = e^{\gamma z/2}[E(-\eta + \sqrt{1-\eta^2})e^{\eta\gamma z/2} + F(\eta + \sqrt{1-\eta^2})e^{-\eta\gamma z/2}]. \tag{18}$$

C. Boundary Conditions

To completely specify our problem, we have to determine the boundary conditions at the PR slab interfaces. To that aim, the Fresnel coefficients at each interface have to be introduced. Let ρ and τ be the reflection and transmission coefficients for an incident electric wave propagating in the air. ρ' and τ' are the reflection and transmission coefficients for an incident electric wave propagating in the PR slab. They can be expressed as functions of the angles θ_0 and θ,

$$\rho(\theta) = -\rho'(\theta) = \frac{\tan(\theta-\theta_0)}{\tan(\theta+\theta_0)},$$

$$\tau(\theta) = \frac{2\cos\theta_0 \sin\theta}{\sin(\theta+\theta_0)\cos(\theta_0-\theta)},$$

$$\tau'(\theta) = \frac{2\cos\theta \sin\theta_0}{\sin(\theta+\theta_0)\cos(\theta-\theta_0)}.$$

The boundary conditions at each interface can be expressed in terms of wave amplitudes,

$$A_3^+(k_\parallel,z=0^+) = \tau A_3^+(k_\parallel,z=0^-) + \rho' A_3^-(k_\parallel,z=0^+), \tag{19}$$

$$A_4^+(-k_\parallel,z=0^+) = \rho' A_4^-(k_\parallel,z=0^+), \tag{20}$$

$$e^{-ik_zL}A_3^-(k_\parallel,z=L) = \rho' e^{ik_zL}A_3^+(k_\parallel,z=L), \tag{21}$$

$$e^{-ik_zL}A_4^-(-k_\parallel,z=L) = \rho' e^{ik_zL}A_4^+(-k_\parallel,z=L). \tag{22}$$

These boundary conditions allow one to determine the constants C, D, E, and F.

D. Reflection and Transmission Coefficients

The analytical solution taking into account absorption losses is too complicated to be shown here. On the contrary, the result is quite simple if we neglect absorption ($a=0$, $\eta=1$). In this case, the transmission and reflection coefficients for the PC process are given by

$$R = \frac{E_4^-(k_\parallel,z=0^-)}{E_3^{+*}(k_\parallel,z=0^-)} = \frac{(1-\rho'^2)^2\sinh(\gamma L/2)\cosh(\gamma L/2)}{(1-\rho'^2)^2\cosh^2(\gamma L/2) + 4\rho'^2\sin^2(k_zL)}, \tag{23}$$

$$T = \frac{E_4^+(k_\parallel,z=L^+)}{E_3^{+*}(k_\parallel,z=0^-)} = \underbrace{\frac{\rho'(1-\rho'^2)\exp(\gamma L/2)\sinh(\gamma L/2)}{(1-\rho'^2)^2\cosh^2(\gamma L/2) + 4\rho'^2\sin^2(k_zL)}}_{=T_0}[e^{jk_zL} - e^{-jk_zL}]. \tag{24}$$

The transmission coefficient T consists of the product of an amplitude term T_0 modulated by the sum of two phase terms $[e^{jk_zL} - e^{-jk_zL}]$ whose origins and consequences will be discussed further. T_0 and R are displayed as functions of the angles θ_0 and α_0 in Fig. 6, considering the coupling coefficient previously shown in Fig. 5. Figure 6(a) shows that internal reflections may allow forward PC (i.e., $T_0 \neq 0$), provided that the coupling coefficient γ is positive (see Fig. 5). This fact can be directly pointed out by considering the asymptotic limits of T_0 [Eq. (24)],

$$\lim_{\gamma L \ll -1} T_0 = \frac{2\rho'}{(1-\rho'^2)}\exp(\gamma L) \to 0, \tag{25}$$

$$\lim_{\gamma L \gg 1} T_0 = \frac{2\rho'}{(1-\rho'^2)} = T_{max} \neq 0. \tag{26}$$

As shown by Fig. 5, γ is positive when $|\alpha_0| > |\theta_0|$. Hence, the best experimental configuration for forward PC is obtained with pump beams grazing the PR slab interfaces. Qualitatively, the need of a positive coupling coefficient can be easily understood. Indeed, if $\gamma < 0$, the probe and conjugated wave fields are exponentially decreasing along the z-axis; hence no phase-conjugated waves can be transmitted through the PR slab. In the case of $BaTiO_3$, the transmission coefficient tends toward a finite value $T_{max} \simeq 1$, for a large PR slab thickness.

Internal reflections have no significant influence on the PC reflectivity. Indeed, it can be easily shown by considering the asymptotic limit of Eq. (23),

$$\lim_{|\gamma L| \gg 1} R = \tanh(\gamma L/2). \tag{27}$$

This last equation is strictly equivalent to the expression of R when internal reflections are neglected [38]. From now on, we will consider an angle of incidence $\alpha_0 = 60°$ for the pump beams. This value is a good compromise between the need for a positive coupling coefficient over the major part of the angular spectrum and experimental feasibility.

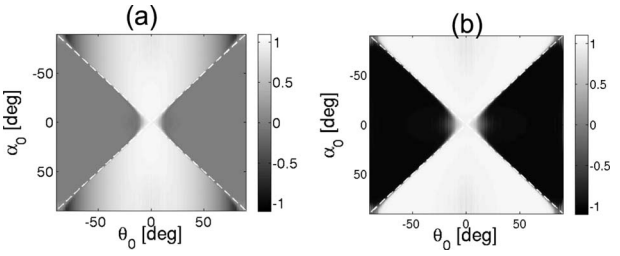

Fig. 6. Evolution of the PC (a) transmission and (b) reflection coefficients as a function of α_0 and θ_0, for $L = 10$ mm.

E. Double Forward PC

Let us now tackle the origin of the phase terms $[e^{ik_zL} - e^{-ik_zL}]$ that appear in the expression of the transmission coefficient T [Eq. (24)]. The forward phase-conjugated wave is generated *via* two different ways (see Fig. 3):

- The probe wave E_3^+ propagates through the PR slab before being reflected at $z=L$. The backward probe wave E_3^- can then be phase-conjugated to give rise to the forward phase-conjugated wave E_4^+. This contribution is associated with the phase term e^{-ik_zL} in Eq. (24).
- The probe wave E_3^+ propagates through the PR slab and is phase-conjugated. The backward phase-conjugated wave E_4^- is then reflected at $z=0$ to give rise to the forward phase-conjugated wave E_4^+. This contribution is associated with the phase term e^{ik_zL} in Eq. (24).

The forward phase-conjugated wave contains two contributions, each one exhibiting a different phase term and hence focusing at different depths (see Fig. 3). We refer to this phenomenon as double forward PC.

Let us now investigate the consequence of double forward PC on imaging. Figure 7 displays the simulation of an experiment consisting of a PR slab placed at $z=0$. Suppose that an opaque screen containing a diffracting structure is introduced in the plane $z=-z_0$. Its amplitude transmittance function $o(\mathbf{r}_\parallel)$ is shown in Fig. 8(a). A plane wave illuminates this diffracting screen and gives rise to a probe wave E_3^+,

$$E_3^+(\mathbf{r}_\parallel, z<0) = \int O(\mathbf{k}_\parallel) e^{i\mathbf{k}_\parallel\cdot\mathbf{r}_\parallel} e^{ik_{z_o}(z+z_0)} \mathrm{d}\mathbf{k}_\parallel, \tag{28}$$

with $O(\mathbf{k}_\parallel)=\int o(\mathbf{r}_\parallel)e^{-i\mathbf{k}_\parallel\cdot\mathbf{r}_\parallel}\mathrm{d}\mathbf{r}_\parallel$. E_3^+ is forward phase-conjugated by the PR slab pumped by (not shown) counter-propagating beams. E_4^+ can be expressed using the transmission coefficient T [Eq. (24)],

$$E_4^+(\mathbf{r}_\parallel, z>L) = \int O(-\mathbf{k}_\parallel) T_0(k_\parallel) e^{-i\mathbf{k}_\parallel\cdot\mathbf{r}_\parallel} e^{i(k_{z_o}(z-L-z_0)+k_zL)} \mathrm{d}\mathbf{k}_\parallel \tag{29}$$

$$- \int O(-\mathbf{k}_\parallel) T_0(k_\parallel) e^{ik_zL} e^{-i\mathbf{k}_\parallel\cdot\mathbf{r}_\parallel} e^{i(k_{z_o}(z-L-z_0)-k_zL)} \mathrm{d}\mathbf{k}_\parallel. \tag{30}$$

The forward phase-conjugated wave E_4^+ is the sum of two contributions [Eqs. (29) and (30)] which give rise to images located at different depths. If the PR slab was transparent ($n=1$, hence $k_z=k_{zo}$), the phase terms in Eqs. (29) and (30) would vanish at $z=z_0$ and $z=z_0+2L$. The image originating from the reflection of E_4^- at $z=0$ would be formed at $z=z_0$ [Eq. (29)]. The one due to the reflection of E_3^+ at $z=L$ would be found at $z=z_0+2L$ [Eq. (30)]. Unfortunately, most non-linear media (and particularly $BaTiO_3$) are not transparent, but one can try to minimize the phase terms in Eqs. (29) and (30). To that aim, the paraxial (or Fresnel) approximation may be used. It consists in considering the Taylor expansions of k_{zo} and k_z until the second order,

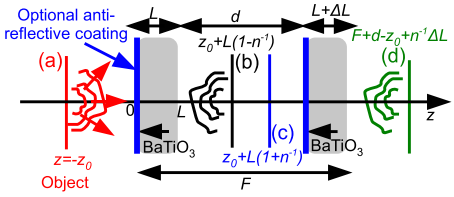

Fig. 7. (Color online) Experimental setup simulated ($\alpha_0=60°$, $L=10$ mm, $\Delta L=0.1$ mm). Both PR slabs are pumped by not shown counter-propagating pump beams (see Fig. 2).

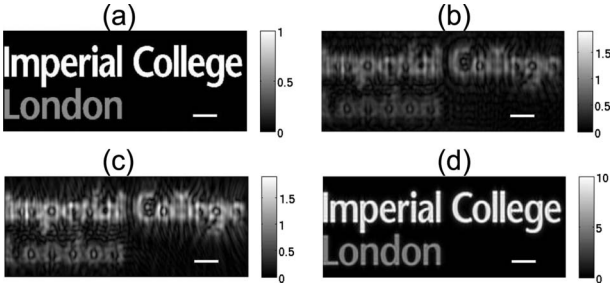

Fig. 8. (a) Transmittance $o(x,y)$ of the opaque screen placed at $z=-z_0$. The white line represents 20λ. (b) Transmitted image by one PCs at $z=z_0+L(1\pm n^{-1})$ [Eqs. (29) and (30)]. (c) Transmitted image by one PCs at $z=z_0+L(1+n^{-1})$ [Eq. (30)] in the presence of an anti-reflective coating and taking into account absorption losses. (d) Transmitted image by two PCs's at $z=F+d-z_0+n^{-1}\Delta L$ [Eq. (54)] taking into account absorption losses and in the presence of anti-reflective coatings.

$$k_z = \sqrt{\left(\frac{n\omega}{c}\right)^2 - k_\parallel^2} \simeq \frac{n\omega}{c} - \frac{k_\parallel^2}{2n\omega/c} + \left(\frac{k_\parallel^4}{4(n\omega/c)^3} + \cdots\right), \tag{31}$$

$$k_{zo} = \sqrt{\left(\frac{\omega}{c}\right)^2 - k_\parallel^2} \simeq \frac{\omega}{c} - \frac{k_\parallel^2}{2\omega/c} + \left(\frac{k_\parallel^4}{4(\omega/c)^3} + \cdots\right). \tag{32}$$

Upon the paraxial approximation, the argument of the phase term in Eqs. (29) and (30) becomes

$$k_{z_o}(z-L-z_0) \pm k_zL = \frac{\omega}{c}(z-z_0-L(1\pm n)) \tag{33}$$

$$- \frac{k_\parallel^2}{2\omega/c}(z-z_0-L(1\pm n^{-1})) \tag{34}$$

$$+ \left(\frac{k_\parallel^4}{4(\omega/c)^3}(z-z_0-L(1\pm n^{-3})) + \cdots\right). \tag{35}$$

The zeroth-order term (33) is not important since it corresponds to a phase shift that is constant over the whole angular spectrum. On the contrary, the second-order term (34) is crucial and vanishes for $z=z_0+L(1\pm n^{-1})$. One image is thus formed at each of these depths. The corresponding wave field is displayed in Fig. 8(b). The imaging performance is poor in terms of resolution. Actually, the paraxial approximation is valid as long as the fourth-order term (35) can be neglected. The aperture angle θ_{lim} can be deduced from this condition,

$$\theta_{lim} = \arcsin\left[\left(\frac{2\lambda}{L(n^{-1}-n^{-3})}\right)^{1/4}\right]. \tag{36}$$

Only the low spatial frequencies add up coherently; phase distortions subsist for high spatial frequencies. The resolution Δ of the image is thus limited by

$$\Delta \sim \left(\frac{\lambda^3 L(n^{-1} - n^{-3})}{2} \right)^{1/4}. \quad (37)$$

For the experimental conditions we consider in Fig. 7, the aperture angle θ_{lim} is 0.13 rad=7.5° and the resolution Δ is 3.9 μm, i.e., 7.6λ.

3. ADDITION OF AN ANTI-REFLECTIVE COATING

Double forward PC is clearly an issue for 3D imaging since two images are superimposed and can blur each other. This problem can be circumvented by adding an anti-reflective coating on the first interface of the PR slab. In that case, only one forward phase-conjugated wavefront is generated. Moreover, the addition of an anti-reflective coating simplifies the problem: analytical expressions of the transmission and reflection coefficients can be derived in the presence of absorption and allow one to study its influence on the PC process.

A. New Transmission and Reflection Coefficients

The addition of an anti-reflective coating on the interface $z=0$ of the PR slab modifies the boundary conditions,

$$A_3^+(k_\parallel, z=0^+) = \tau_0 A_3^+(k_\parallel, z=0^-), \quad (38)$$

$$A_4^+(-k_\parallel, z=0^+) = 0. \quad (39)$$

$\tau_0 = n^{-1/2}$ and $\tau_0' = n^{1/2}$ are the transmission coefficients through the anti-reflective coating. These boundary conditions plus the ones at the interface $z=L$ [Eqs. (21) and (22)] allow one to determine the constants C, D, E, and F of Eqs. (15)–(18). New transmission and reflection coefficients, R^{ac} and T^{ac}, are deduced in the presence of an anti-reflective coating,

$$R^{ac} = \frac{[(1-\rho'^2)\eta \cosh(\eta\gamma L/2) + (1+\rho'^2)\sqrt{1-\eta^2}\sinh(\eta\gamma L/2)]\sinh(\eta\gamma L/2)}{(1-\rho'^2(2\eta^2-1))\sinh^2(\eta\gamma L/2) + \eta\sqrt{1-\eta^2}\sinh(\eta\gamma L) + \eta^2}, \quad (40)$$

$$T^{ac} = \underbrace{-\frac{\tau_0\tau'\rho'\eta \exp(\gamma L/2)\sinh(\eta\gamma L/2)}{(1-\rho'^2(2\eta^2-1))\sinh^2(\eta\gamma L/2) + \eta\sqrt{1-\eta^2}\sinh(\eta\gamma L) + \eta^2}}_{=T_0^{ac}} e^{-ik_z L}. \quad (41)$$

The transmission coefficient T^{ac} now consists of a product of an amplitude term T_0^{ac} only modulated by the phase term $e^{-jk_z L}$. Only the forward phase-conjugated wave corresponding to the reflection on the interface $z=L$ subsists. The one linked with the reflection at $z=0$ is cancelled out by the anti-reflective coating.

B. Effect of Absorption

T_0^{ac} and R^{ac} are displayed as functions of the angles θ_0 and L in Fig. 9, considering the coupling coefficient γ shown in Fig. 5. γ is positive when $|\theta_0| < |\alpha_0| = 60°$; hence forward PC only occurs over this angular spectrum. Therefore the remaining part of the angular spectrum ($|\theta_0| > |\alpha_0|$) is not shown. Figure 9 illustrates the effect of absorption on forward PC. Not surprisingly, absorption implies a less efficient PC process both in transmission and reflection. This fact can be directly pointed out by considering the asymptotic limits of R^{ac} and T_0^{ac} for $\alpha' \ll \gamma$,

$$\lim_{\gamma L \gg 1} R^{ac} \underset{\alpha' \ll \gamma}{\sim} \frac{\eta}{1 + \frac{2(1-\eta^2)}{1-\rho'^2}} = \beta < 1, \quad (42)$$

$$\lim_{\gamma L \gg 1} T_0^{ac} \underset{\alpha' \ll \gamma}{\sim} \frac{\tau'\tau_0\rho'}{(1-\rho'^2)} \beta e^{\gamma(1-\eta)L} = T_{max}^{ac}. \quad (43)$$

For $\gamma L \gg 1$, absorption comes to multiply the reflection coefficient by a factor $\beta < 1$. Hence, the reflectivity of a PCs no longer approaches unity in the presence of absorption [see the comparison between Figs. 9(c) and 9(d)]. This fact will be particularly important when the combination of two PCs's will be investigated (see Section 4). In transmission, the effect of absorption is more unexpected. The term $e^{\gamma(1-\eta)L}$ in Eq. (43) implies that the transmission coefficient can be amplified thanks to absorption. However, this counter-intuitive effect would be possible only for ex-

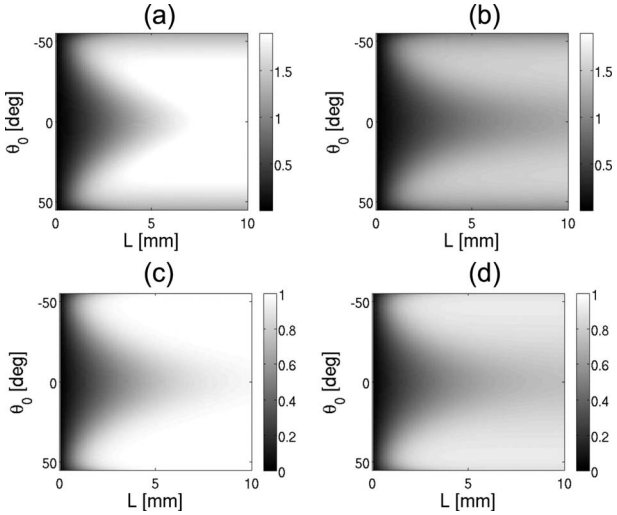

Fig. 9. Evolution of T_0^{ac} as a function of L and θ_0 (a) neglecting or (b) taking into account absorption. Evolution of R^{ac} as a function of L and θ_0 (c) neglecting or (d) taking into account absorption.

tremely large thickness L, such that $\beta e^{\gamma(1-\eta)L} > 1$. The comparison between Figs. 9(a) and 9(b) shows the effect of absorption in transmission for a range of thicknesses L generally used in the FWM experiment. In this regime, the transmission coefficient is clearly diminished by the absorption losses. However, note that despite absorption the system is able of amplification in transmission: $T^{ac}_{max} \simeq 1.5$. Note that this would not be true if the anti-reflective coating was added on the second interface ($z=L$): a part of the probe wave would be reflected at the first interface and would not take part in the PC process. In that case, $T^{ac}_{max} = 2\tau\tau'_0\rho'/(1-\rho'^2)\beta e^{\gamma(1-\eta)L} \simeq 0.35 < 1$. Thus, the best experimental configuration for forward PC is to add the anti-reflective coating on the first interface ($z=0$).

C. Imaging Performance

Contrary to its previous expression [Eq. (24)], the transmission coefficient now only exhibits the phase term $e^{-ik_z L}$. Therefore, an object placed at $z=-z_0$ would no longer be associated with two images but only with the one formed at $z=z_0+L(1+n^{-1})$. Let us investigate the imaging performance of the PR slab in the presence of an anti-reflective coating. To that aim, the experiment shown in Fig. 7 is simulated with an anti-reflective coating at $z=0$. The image obtained at $z=z_0+L(1+n^{-1})$ is shown in Fig. 8(c). The imaging performance is better in terms of contrast [see the comparison with Fig. 8(b)]. However, the resolving power is still limited by the phase distortions at high spatial frequencies [Eq. (37)].

4. COMBINATION OF TWO PHASE CONJUGATORS

Now that the possibility of performing forward PC has been investigated theoretically, the issue of combining two PCs's is addressed. The transmission coefficient of the whole system is first derived. The device is shown to be analogous to a resonant cavity: the wave field can be amplified by a factor of 10^2 in intensity despite absorption losses. As to imaging purposes, the second PCs is shown to automatically compensate the phase distortions undergone by the forward phase-conjugated wave-front at the first PCs. Thus, the resolving power of the device is drastically improved: the aperture angle θ_{lim} is no longer limited by the thickness L of the PCs [Eq. (36)] but only by the difference of thickness ΔL between the two PCs.

A. Transmission Coefficient of the Overall System

The principle of a lens combining two PCs's is shown in Fig. 10. The system is composed of two PCs's of thicknesses L_a and L_b separated by a distance d. An anti-reflective coating is added on the first interface of each PCs. This is the best configuration since it provides a more efficient forward PC process ($|T_a|, |T_b| > 1$). Keep also in mind that the two PCs's are pumped by (not shown) counter-propagating pump beams (see Fig. 2). The problem is solved by considering an incident p-polarized plane wave $\mathbf{\Psi_0}(\mathbf{k}_\parallel)$, such that

$$\mathbf{\Psi_0}(\mathbf{k}_\parallel, z<0) = \psi_0(\mathbf{k}_\parallel) e^{ik_{z_0} z} e^{i\mathbf{k}_\parallel \cdot r_\parallel} \hat{\mathbf{e}}_{\theta_0}.$$

Between the two PCs's, the phase-conjugated wave field consists of a forward going wave $\mathbf{\Psi_1}$ and a backward going one $\mathbf{\Psi_3}$,

$$\mathbf{\Psi_1}(-\mathbf{k}_\parallel, L_a < z < d+L_a) = \psi_1(-\mathbf{k}_\parallel) e^{ik_{z_0}(z-L_a)} e^{-i\mathbf{k}_\parallel \cdot r_\parallel} \hat{\mathbf{e}}_{-\theta_0},$$

$$\mathbf{\Psi_3}(\mathbf{k}_\parallel, L_a < z < d+L_a) = \psi_3(\mathbf{k}_\parallel) e^{-ik_{z_0}(z-L_a)} e^{i\mathbf{k}_\parallel \cdot r_\parallel} \hat{\mathbf{e}}_{-\theta_0}.$$

The wave $\mathbf{\Psi_2}$ transmitted through the device can be expressed as

$$\mathbf{\Psi_2}(\mathbf{k}_\parallel, z>F) = \psi_2(\mathbf{k}_\parallel) e^{ik_{z_0}(z-F)} e^{i\mathbf{k}_\parallel \cdot r_\parallel} \hat{\mathbf{e}}_{\theta_0},$$

where $F=d+L_a+L_b$.

To solve this problem, the PC process that occurs at each PCs can be expressed in terms of boundary conditions:

$$\text{1st PCs:} \quad \psi_1(-\mathbf{k}_\parallel) = T_a(k_\parallel)\psi_0^*(\mathbf{k}_\parallel) + R_a(k_\parallel)\psi_3^*(\mathbf{k}_\parallel), \tag{44}$$

$$\text{2nd PCs:} \quad \psi_3(\mathbf{k}_\parallel) e^{-ik_{z_0} d} = R_b(k_\parallel)[\psi_1(-\mathbf{k}_\parallel) e^{ik_{z_0} d}]^*, \tag{45}$$

$$\psi_2(\mathbf{k}_\parallel) = T_b(k_\parallel)[\psi_1(-\mathbf{k}_\parallel) e^{ik_{z_0} d}]^*. \tag{46}$$

This system is easily solved and the transmitted field $\mathbf{\Psi_2}$ can be expressed as

$$\mathbf{\Psi_2}(\mathbf{k}_\parallel, z>F) = T_2(k_\parallel)\psi_0(\mathbf{k}_\parallel) e^{i\mathbf{k}_\parallel \cdot r_\parallel} e^{ik_{z_0}(z-F-d)} \hat{\mathbf{e}}_{\theta_0}, \tag{47}$$

with

$$T_2(k_\parallel) = \frac{T_a^*(-k_\parallel) T_b(k_\parallel)}{1 - R_a^*(-k_\parallel) R_b(k_\parallel)}. \tag{48}$$

$T_2(k_\parallel)$ is the transmission coefficient of the overall system. Its numerator $T_a^*(-k_\parallel)T_b(k_\parallel)$ represents the two successive forward PC operations undergone by the wave-front. Its denominator $1-R_a^*(-k_\parallel)R_b(k_\parallel)$ comes from the multiple scattering loop between the two PCs.

B. A Lens Combining Two PCs Acts as a Resonant Cavity

For the sake of simplicity, let us assume for the moment that the two PCs's are of the same thickness $L=L_a=L_b$. Hence, $T=T_a=T_b$ and $R=R_a=R_b$. T_2 becomes

$$T_2(k_\parallel) = \frac{|T(k_\parallel)|^2}{1 - |R(k_\parallel)|^2}. \tag{49}$$

The first observation is that T_2 is real and positive which means that the phase distortions observed previously for high spatial frequencies are completely removed when

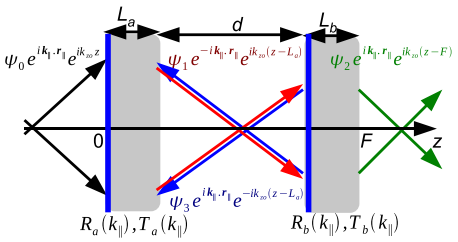

Fig. 10. (Color online) Scheme describing the different waves propagating when two PCs's are placed in front of each other.

two PCs's are combined. This is a promising perspective for imaging purposes (see Subsection 4C). Second, the combination of two PCs's provides a significant amplification of the wave field. This gain would be theoretically infinite in the absence of absorption since the PC reflectivity tends toward unity for $\gamma L \gg 1$. The system is then analogous to a resonant cavity,

$$\lim_{\gamma L \gg 1} R(k_\parallel) = 1 \Rightarrow \lim_{\gamma L \gg 1} T_2(k_\parallel) = \infty. \tag{50}$$

Of course, absorption losses limit this amplification in practice. Figure 11 displays T_2 [Eq. (49)] as a function of θ_0 considering the transmission and reflection coefficients previously derived in the presence of absorption [Eqs. (40) and (41)]. Despite these losses, the system is still able of amplification. For $L=10$ mm, the device exhibits a gain of 10^2 in intensity. The transmission coefficient T_2 varies as a function of the angle of incidence θ_0 from 5 ($\theta=0°$) to 10 ($\theta=50°$). This variation is sufficiently moderate to not affect the imaging fidelity of the device as we will see in the following.

C. Imaging When Two PCs's Are Combined

Let us see the imaging performance of a lens combining two PCs's. To that aim, the experiment shown in Fig. 10 is simulated. The diffracting screen placed at $z=-z_0$ is displayed in Fig. 8(a). The field ψ_2 at the device output can be expressed using Eq. (47) as

$$\psi_2(\mathbf{r}_\parallel, z > F) = \int O(\mathbf{k}_\parallel) T_2(k_\parallel) e^{i\mathbf{k}_\parallel \cdot \mathbf{r}_\parallel} e^{ik_{z_0}(z+z_0-F-d)} d\mathbf{k}_\parallel. \tag{51}$$

The transmission coefficients $T_{a,b}$ of each individual PCs can be expressed as the product of an amplitude and a phase term,

$$T_{a,b}(k_\parallel) = -T_{0,a,b}(k_\parallel) e^{-ik_z L_{a,b}}. \tag{52}$$

The transmission function T_2 [Eq. (48)] can be expressed in the same way as

$$T_2(k_\parallel) = \underbrace{\frac{T_{0,a}(-k_\parallel) T_{0,b}(k_\parallel)}{1 - R_a(-k_\parallel) R_b(k_\parallel)}}_{T_{0,2}(k_\parallel)} e^{-ik_z \Delta L}, \tag{53}$$

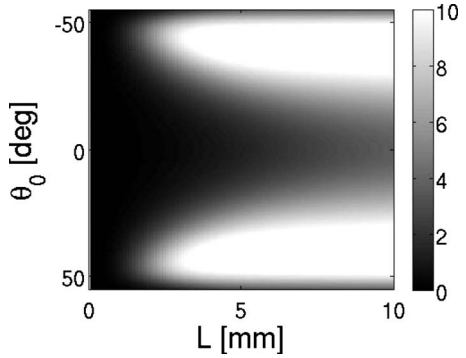

Fig. 11. Evolution of T_2 as a function of L and θ_0 for two PCs's of the same thickness ($L=10$ mm, $\alpha_0=60°$).

with $\Delta L = L_b - L_a$. This expression of T_2 can be substituted into Eq. (51),

$$\psi_2(\mathbf{r}_\parallel, z > d+F) = \int O(\mathbf{k}_\parallel) T_{0,2}(k_\parallel) e^{i\mathbf{k}_\parallel \cdot \mathbf{r}_\parallel} e^{ik_{z_0}(z+z_0-F-d)} e^{-ik_z \Delta L} d\mathbf{k}_\parallel. \tag{54}$$

If both PR slabs are strictly of the same thickness ($\Delta L = 0$), then $T_2 = T_{0,2}$ is real and positive. The second PCs automatically compensates the phase distortions undergone by the forward phase-conjugated wave-front at the first PCs. An undistorted image is then obtained at the depth $d+F-z_0$. The resolving power of the device is only limited by the classical limit of diffraction.

However, the two PCs's will never be of the same thickness in practice. In that case, the phase distortions are only partially compensated by the second PCs. These residual distortions appear in Eq. (53) through the term $e^{-ik_z \Delta L}$. As illustrated in Fig. 12, they lead to a displacement of the focal point. To know the image location, the phase term in Eq. (54) has to be minimized. To that aim, we can proceed as in Subsection 2E, replacing L with ΔL. Under the paraxial approximation, one can show that the image is formed at the depth $z = F + d - z_0 + n^{-1}\Delta L$. The condition of validity for the paraxial approximation allows one then to deduce the aperture angle θ_{lim} and the resolution Δ of the image,

$$\theta_{lim} \sim \arcsin\left[\left(\frac{2\lambda}{\Delta L(n^{-1} - n^{-3})}\right)^{1/4}\right], \tag{55}$$

$$\Delta \sim \left(\frac{\lambda^3 \Delta L(n^{-1} - n^{-3})}{2}\right)^{1/4}. \tag{56}$$

The imaged wave field is displayed in Fig. 8(d) for a difference of thickness $\Delta L = 0.1$ mm between the two PCs's. The object pattern is nicely recovered. Actually, the aperture angle θ_{lim} is, in this case, 0.4 rad=23.5° and the resolution Δ is 1.25 μm, i.e., 2.4λ. The addition of a second PCs significantly improve the resolving power of the device since Δ now depends on ΔL [Eq. (37)] instead of the thickness L itself [Eq. (56)]. The comparison between Figs. 8(c) and 8(d) illustrates the gain in resolution provided by the combination of two PCs's. Note also the amplification of the imaged wave field by a factor of 10^2 in intensity [Fig. 8(d)], as predicted in Subsection 4B.

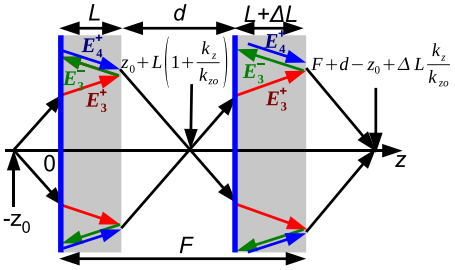

Fig. 12. (Color online) Scheme describing the paths taken by the partial waves inside the non-linear slabs when two PCs's are associated.

5. CONCLUSION

In this study, we have proposed an experimental setup to mimic negative refraction in the optical regime *via* PC. This is performed by means of FWM in a PR slab made of $BaTiO_3$. We have shown how to take advantage of internal reflections inside the PR slab to perform simultaneously backward and forward PC. The experimental conditions needed to obtain an efficient and uniform PC process over the whole angular spectrum have been determined (orientation of the c-axis along $-z$, extraordinary polarizations, and large angle of incidence for the pump beams). Double forward PC has been predicted: the wave reflections on each PR slab interface gives rise to two forward phase-conjugated wave-fronts, focusing at different depths. A superposition of two images, separated by a distance $2n^{-1}L$, is thus obtained. This is an issue for 3D imaging since each image may blur the other one. A solution is to add an anti-reflective coating on the first interface of the PR slab. Satisfying imaging is then obtained upon the paraxial approximation. However, phase distortions are shown to subsist for high spatial frequency components, which limits the resolving power of the device [Eq. (37)].

On the contrary, the combination of two PCs's offers promising features for imaging purposes. The second PCs is shown to automatically compensate the phase distortions undergone by the forward phase-conjugated wavefront at the first PCs. The aperture angle of the system is only limited by the difference of thickness ΔL between the two phase conjugators. The propagating wave field is perfectly translated through the device, hence mimicking a negative refractive slab at optical frequencies. Actually, the combination of two PCs's performs even better than negative refraction. The two PCs's are shown to behave like a resonant cavity: in theory, the wave field could be amplified infinitely since the two PCs's exhibit a reflectivity close to unity. However, absorption losses limit this amplification process in practice. The effect of absorption on the PC process has been investigated analytically and an amplification of the wave field by a factor of 10^2 in intensity is predicted, despite the important absorption in $BaTiO_3$.

As claimed in the introduction, mimicking a negative refractive slab by combining two phase conjugators would be of considerable interest since such a device would constitute an *absolute* optical instrument [17]. Besides opening a new route toward 3D imaging, it may also provide a significant amplification of the imaged wave field. The perspective of this work is, of course, to implement in practice the experimental setup suggested by our theoretical study. As to sub-wavelength imaging [11], the question remains open and depends on a future breakthrough in surface non-linear optics.

APPENDIX: THEORETICAL EXPRESSION OF THE COUPLING COEFFICIENT

This appendix is dedicated to the theoretical calculation of the coupling coefficient γ. The experimental configuration is described in Fig. 2. In this appendix, only the PC process between the probe wave $\mathbf{E_3^+}$ and the backward phase-conjugated wave $\mathbf{E_4^-}$ is addressed. In our experimental configuration, the PR slab is pumped by two couples of counter-propagating pump beams. Hence two FWM processes occur simultaneously. One is associated with the pump beams $\mathbf{E_1^+}$ and $\mathbf{E_2^+}$ and is characterized by a coupling coefficient γ^+; the other one is associated with $\mathbf{E_1^-}$ and $\mathbf{E_2^-}$ and characterized by a coupling coefficient γ^-. In this appendix, we will establish the theoretical expression of γ^+. Then, the overall coupling coefficient γ will be deduced by simple geometric arguments.

A. The Grating Formation Process

The PR crystal is illuminated by an intensity distribution $I(\mathbf{r})$ due to the interference between the pump beams and the probe and conjugated waves,

$$I(\mathbf{r}) = I_0 + [I_I \exp(i\mathbf{k_I}\cdot\mathbf{r}) + \text{c.c.}] + [I_{II} \exp(i\mathbf{k_{II}}\cdot\mathbf{r}) + \text{c.c.}], \tag{A1}$$

where $I_0 = \Sigma_{j=1}^4 |A_j|^2$ is the total intensity. The undepleted pump approximation means that the intensity of pumps beams is much stronger than the probe and conjugate beam intensities. Hence $I_0 \simeq |A_1|^2 + |A_2|^2$. I_1 represents the amplitude of the interference pattern between beams 1/2 and 3/4,

$$I_I = (A_1^* A_3^+ + A_4^{-*} A_2)\cos(\alpha - \theta). \tag{A2}$$

The corresponding grating vector is $\mathbf{k_I} = \mathbf{k} - \mathbf{q} = k_1 \mathbf{u_1}$, with $\mathbf{u_I} = -\cos[(\alpha+\theta)/2]\mathbf{u_x} + \sin[(\alpha+\theta)/2]\mathbf{u_z}$ (see Fig. 13). I_{II} represents the amplitude of the interference pattern between beams 1/2 and 4/3,

$$I_{II} = (A_4^{-*} A_1 + A_2^* A_3^+)\cos(\alpha - \theta). \tag{A3}$$

The associated grating vector is $\mathbf{k_{II}} = \mathbf{k} + \mathbf{q} = k_{II}\mathbf{u_{II}}$, with $\mathbf{u_{II}} = \sin[(\alpha+\theta)/2]\mathbf{u_x} + \cos[(\alpha+\theta)/2]\mathbf{u_z}$ (see Fig. 13).

The intensity distribution $I(\mathbf{r})$ excites charges (electrons or holes) into a conduction band, where it migrates by diffusion and drift. In the absence of an externally applied electric field, the electric field E^{sc} associated with the resultant space charge distribution can be expressed as [46,51]

$$\mathbf{E^{sc}}(\mathbf{r}) = [E_I^{sc} \exp(i\mathbf{k_I}\cdot\mathbf{r}) + \text{c.c.}]\mathbf{u_I} + [E_{II}^{sc} \exp(i\mathbf{k_{II}}\cdot\mathbf{r}) + \text{c.c.}]\mathbf{u_{II}}. \tag{A4}$$

The resultant electric field $\mathbf{E^{sc}}$ is the sum of two components originating from each interference pattern. The relation between the electric field amplitude $E_{I,II}^{sc}$ and the interference pattern amplitude $I_{I,II}$ is [46,51]

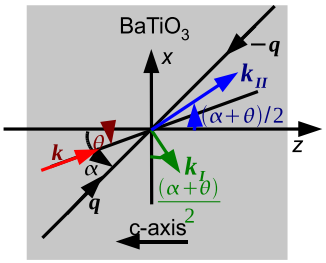

Fig. 13. (Color online) Grating vectors $\mathbf{k_I}$ and $\mathbf{k_{II}}$.

$$E_{I,II}^{sc} = -i\frac{I_{I,II}}{I_0}\frac{E_{I,II}^{d}}{1+E_{I,II}^{d}/E_{I,II}^{p}}. \tag{A5}$$

E^d and E^p are electric fields characteristic of diffusion and maximum space charge, respectively,

$$E_{I,II}^{d} = \frac{k_B T k_{I,II}}{e}, \quad E_{I,II}^{p} = \frac{eN_A}{\epsilon_{eff,I,II}^{S} k_{I,II}}, \tag{A6}$$

where k_B is the Boltzmann constant, T is the temperature, e is the electron charge, N_A is the acceptor density, and ϵ_{eff}^{S} is the effective static permittivity (or dielectric constant).

The last step of the hologram writing process is the grating formation. The electric field operates through the electro-optic effect to modulate the index of refraction. The change in permittivity ϵ due to an electric field $\mathbf{E^{sc}}$ is given by

$$\Delta\epsilon_{ij} = -\epsilon_{ii} r_{ijk} E_k^{sc} \epsilon_{jj}, \tag{A7}$$

where $\mathbf{R}=r_{ijk}$ is the electro-optic tensor. For crystals of the point group 4 mm such as $BaTiO_3$, the non-zero electro-optic coefficients and their conventional contracted notations are $r_{www}\equiv r_{33}$, $r_{uuw}\equiv r_{13}$, and $r_{uwu}\equiv r_{42}$.The directions (u,v,w) are the principal dielectric axes, with w aligned along the direction of the c-axis. In our configuration, the crystal axis is in the opposite direction to the z-axis; hence $(u,v,w)=(-x,y,-z)$. A simplified expression of the permittivity variation tensor $\boldsymbol{\Delta\epsilon}$ can be derived from Eq. (A7),

$$\boldsymbol{\Delta\epsilon} = \begin{pmatrix} n_o^4 r_{13} E_z^{sc} & n_o^2 n_e^2 r_{42} E_x^{sc} \\ n_o^2 n_e^2 r_{42} E_x^{sc} & n_e^4 r_{33} E_z^{sc} \end{pmatrix}. \tag{A8}$$

If we inject the expression of the space charge field $\mathbf{E^{sc}}$ [Eq. (A4)], $\boldsymbol{\Delta\epsilon}$ can be derived as the sum of two components associated with the transmission and the reflection gratings, respectively,

$$\boldsymbol{\Delta\epsilon} = \boldsymbol{\Delta\epsilon_I} e^{i\mathbf{k_I}\cdot\mathbf{r}} + \boldsymbol{\Delta\epsilon_{II}} e^{i\mathbf{k_{II}}\cdot\mathbf{r}} + \text{c.c.} \tag{A9}$$

B. Coupled Wave Equations

We now tackle the reading step. To that aim, we consider the scalar wave equation that the probe and conjugate plane waves are supposed to verify along their directions of polarization $\hat{\mathbf{e}}_\theta$,

$$\Delta(E_3^+ + E_4^-) + \left(\frac{n\omega}{c}\right)^2 (E_3^+ + E_4^-) = -\frac{\omega^2}{c^2}[\hat{\mathbf{e}}_\theta \cdot \boldsymbol{\Delta\epsilon} \cdot \hat{\mathbf{e}}_\alpha](E_1^+ + E_2^+). \tag{A10}$$

The source term that appears on the right of the last equation denotes the reading of the hologram by the pump beams E_1 and E_2. Substituting expressions of the wave fields E_j and of $\boldsymbol{\Delta\epsilon}$ [Eq. (A9)] in Eq. (A10), recognizing that $k=n\omega/c$, neglecting the second derivative terms compared to those involving the first derivatives, and equating separately synchronous terms with the same exponential factors lead to the coupled wave equations [46],

$$\frac{dA_3^+}{dz} = \frac{\gamma_I^+}{I_0}(A_1^* A_3^+ + A_2 A_4^{-*})A_1 + \frac{\gamma_{II}^+}{I_0}(A_1 A_4^{-*} + A_2^* A_3^+)A_2, \tag{A11}$$

$$\frac{dA_4^-}{dz} = \frac{\gamma_I^+}{I_0}(A_1 A_3^{+*} + A_2^* A_4^-)A_2 + \frac{\gamma_{II}^+}{I_0}(A_1^* A_4^- + A_2 A_3^{+*})A_1. \tag{A12}$$

The real coupling coefficients $\gamma_{I,II}^+$ are given by

$$\gamma_{I,II}^+ = -\frac{\omega}{2nc\cos\theta}\frac{r_{I,II}E_{I,II}^{d}}{1+E_{I,II}^{d}/E_{I,II}^{p}}\cos(\alpha-\theta), \tag{A13}$$

where $r_{I,II}$ are the effective electro-optic coefficients,

$$\begin{aligned} r_I = &-n_o^4 r_{13}\sin\left(\frac{\alpha+\theta}{2}\right)\cos\alpha\cos\theta \\ &- n_o^2 n_e^2 r_{42}\cos\left(\frac{\alpha+\theta}{2}\right)\sin(\alpha+\theta) \\ &- n_e^4 r_{33}\sin\left(\frac{\alpha+\theta}{2}\right)\sin\alpha\sin\theta, \end{aligned} \tag{A14}$$

$$\begin{aligned} r_{II} = &-n_o^4 r_{13}\cos\left(\frac{\alpha+\theta}{2}\right)\cos\alpha\cos\theta \\ &+ n_o^2 n_e^2 r_{42}\sin\left(\frac{\alpha+\theta}{2}\right)\sin(\alpha+\theta) \\ &- n_e^4 r_{33}\cos\left(\frac{\alpha+\theta}{2}\right)\sin\alpha\sin\theta. \end{aligned} \tag{A15}$$

The problem can then be simplified assuming that the two pump intensities are of equal intensities: $|A_1|^2=|A_2|^2=I_0/2$. The coupled wave equations reduce to

$$\frac{dA_3^{+*}}{dz} - \frac{\gamma^+}{2}A_3^{+*} = \frac{\gamma^+}{2}e^{-i\phi}A_4^-, \tag{A16}$$

$$\frac{dA_4^-}{dz} - \frac{\gamma^+}{2}A_4^- = \frac{\gamma^+}{2}e^{i\phi}A_3^{+*}, \tag{A17}$$

with $\gamma^+=\gamma_I^+ + \gamma_{II}^+$ and $e^{i\phi}=2A_1A_2/I_0$. In our study, we assume that $\phi=\pi$, i.e., $A_1=-A_2$. This is the case experimentally if one pump beam is obtained by reflection of the other pump beam on a silvered mirror.

C. Overall Coupling Coefficient

In our study, we assume that a second couple of counterpropagating pump beams $\mathbf{E_1^-}$ and $\mathbf{E_2^-}$, symmetric to the first one (i.e., with an angle of incidence $-\alpha$), is added (see Fig. 2). This couple of pump beams also interacts with the probe wave to give rise to the phase-conjugated wave. The associated coupling coefficient γ^- can be expressed simply as a function of γ^+, such that

$$\gamma^-(\theta,\alpha) = \gamma^+(\theta,-\alpha). \tag{A18}$$

Finally, assuming that all pump beams are of equal intensities, the PC process between $\mathbf{E}_3^+$ and $\mathbf{E}_4^-$ taking place in the PR slab can be modeled by an overall coupling coefficient γ, such that

$$\gamma(\theta,\alpha) = \gamma^+(\theta,\alpha) + \gamma^-(\theta,\alpha) = \gamma^+(\theta,\alpha) + \gamma^+(\theta,-\alpha). \tag{A19}$$

ACKNOWLEDGMENTS

The authors wish to thank Mickael Damzen for fruitful discussions. This work was supported by the European Community project PHOME (contract No. 213390).

REFERENCES

1. J. B. Pendry, "Negative refraction makes a perfect lens," Phys. Rev. Lett. **85**, 3966–3969 (2000).
2. S. A. Ramakrishna, "Physics of negative refractive index materials," Rep. Prog. Phys. **68**, 449–521 (2005).
3. C. M. Soukoulis, M. Kafesaki, and E. N. Economou, "Negative-index materials: new frontiers in optics," Adv. Mater. **18**, 1941–1952 (2006).
4. G. V. Eleftheriades and K. G. Balmain, *Negative-Refraction Metamaterials: Fundamental Principles and Applications* (Wiley-IEEE, 2005).
5. V. G. Veselago, "The electrodynamics of substances with simultaneously negative values of ϵ and μ," Sov. Phys. Usp. **10**, 509–514 (1968).
6. A. Grbic and G. V. Eleftheriades, "Overcoming the diffraction limit with a planar left-handed transmission-line lens," Phys. Rev. Lett. **92**, 117403 (2004).
7. N. Fang, H. Lee, C. Sun, and X. Zhang, "Sub-diffraction-limited optical imaging with a silver superlens," Science **308**, 534–537 (2005).
8. J. T. Shen and P. M. Platzman, "Near field imaging with negative dielectric constant lenses," Appl. Phys. Lett. **80**, 3286–3288 (2002).
9. D. R. Smith, D. Schurig, M. Rosenbluth, S. Schultz, S. A. Ramakrishna, and J. B. Pendry, "Limitations on subdiffraction imaging with a negative refractive index slab," Appl. Phys. Lett. **82**, 1506–1508 (2003).
10. Z. Ye, "Optical transmission and reflection of perfect lenses by left handed materials," Phys. Rev. B **67**, 193106 (2003).
11. J. B. Pendry, "Time reversal and negative refraction," Science **322**, 71–73 (2008).
12. M. Nieto-Vesperinas and E. Wolf, "Phase conjugation and symmetries with wave fields in free space containing evanescent components," J. Opt. Soc. Am. A **2**, 1429–1434 (1985).
13. S. Maslovski and S. Tretyakov, "Phase conjugation and perfect lensing," J. Appl. Phys. **94**, 4241–4243 (2003).
14. S. I. Bozhevolnyi, O. Keller, and I. I. Smolyaninov, "Phase conjugation of an optical near field," Opt. Lett. **19**, 1601–1603 (1994).
15. S. I. Bozhevolnyi, O. Keller, and I. I. Smolyaninov, "Scattered light enhancement near a phase conjugating mirror," Opt. Commun. **115**, 115–120 (1995).
16. B. Vohnsen and S. I. Bozhevolnyi, "Near-field optical microscopy with a phase-conjugating mirror," Opt. Commun. **148**, 331–337 (1998).
17. M. Born and E. Wolf, *Principle of Optics* (Pergamon, 1980).
18. A. L. Pokrovsky and A. L. Efros, "Diffraction theory and focusing of light by a slab of left-handed material," Physica B **338**, 333–337 (2003).
19. R. W. Hellwarth, "Generation of time-reversed wave fronts by nonlinear refraction," J. Opt. Soc. Am. **67**, 1–3 (1977).
20. A. Yariv, "Phase conjugation," IEEE J. Quantum Electron. **14**, 650–660 (1978).
21. R. Fisher, *Optical Phase Conjugation* (Academic, 1984).
22. G. S. He, "Optical phase conjugation: principles, techniques, and applications," Prog. Quantum Electron. **26**, 131–191 (2002).
23. D. M. Bloom and G. C. Bjorklund, "Conjugate wave-front generation and image reconstruction by four-wave mixing," Appl. Phys. Lett. **31**, 592–594 (1977).
24. D. M. Bloom, P. F. Liao, and N. P. Economou, "Observation of amplified reflection by degenerate four-wave mixing in atomic sodium vapor," Opt. Lett. **2**, 58–60 (1978).
25. D. M. Pepper, D. Fekete, and A. Yariv, "Observation of amplified phase-conjugate reflection and optical parametric oscillation by degenerate four-wave mixing in a transparent medium," Appl. Phys. Lett. **33**, 41–44 (1978).
26. D. Fekete, J. C. AuYeung, and A. Yariv, "Phase-conjugate reflection by degenerate four-wave mixing in a nematic liquid crystal in the isotropic phase," Opt. Lett. **5**, 51–53 (1980).
27. R. L. Abrams and R. C. Lind, "Degenerate four wave mixing in absorbing media," Opt. Lett. **2**, 94–96 (1978).
28. A. Tomita, "Phase conjugation using gain saturation of a Nd:YAG laser," Appl. Phys. Lett. **34**, 463–464 (1979).
29. R. A. Fisher and B. J. Feldman, "On-resonant phase-conjugate reflection and amplification at 10.6 μm in inverted CO_2," Opt. Lett. **4**, 140–142 (1979).
30. Y. Silberberg and I. Bar-Joseph, "Low power phase conjugation in thin films of saturable absorbers," Opt. Commun. **39**, 265–268 (1981).
31. G. J. Crofts, R. P. M. Green, and M. J. Damzen, "Investigation of multipass geometries for efficient degenerate four-wave mixing in Nd:YAG," Opt. Lett. **17**, 920–922 (1992).
32. M. J. Damzen, R. P. M. Green, and G. J. Crofts, "High-reflectivity four-wave mixing by gain saturation of nanosecond and microsecond radiation in Nd:YAG," Opt. Lett. **17**, 1331–1333 (1992).
33. K. S. Syed, G. J. Crofts, R. P. M. Green, and M. J. Damzen, "Vectorial phase conjugation via four-wave mixing in isotropic saturable-gain media," J. Opt. Soc. Am. B **14**, 2067–2078 (1997).
34. J. Feinberg, D. Heiman, J. A. R. Tanguay, and R. W. Hellwarth, "Photorefractive effects and light-induced charge migration in barium titanate," J. Appl. Phys. **51**, 1297–1305 (1980).
35. J. P. Huignard, J. P. Herriau, P. Aubourg, and E. Spitz, "Phase-conjugate wavefront generation via real-time holography in $Bi_{12}SiO_{20}$ crystals," Opt. Lett. **4**, 21–23 (1979).
36. J. Feinberg and R. W. Hellwarth, "Phase-conjugating mirror with continuous-wave gain," Opt. Lett. **5**, 519–521 (1980).
37. J. O. White, M. Cronin-Golomb, B. Fischer, and A. Yariv, "Coherent oscillation by self-induced gratings in the photorefractive crystal $BaTiO_3$," Appl. Phys. Lett. **40**, 450–452 (1982).
38. M. Cronin-Golomb, B. Fisher, J. O. White, and A. Yariv, "Theory and applications of four-wave mixing in photorefractive media," IEEE J. Quantum Electron. **20**, 12–30 (1984).
39. P. Günter and J.-P. Huignard, *Photorefractive Materials and Their Applications I* (Springer-Verlag, 1988).
40. A. Khyznika, V. Kondilenko, Y. Kucherov, S. Lesnik, S. Odoulov, and M. Soskin, "Phase conjugation by degenerate forward four-wave mixing," J. Opt. Soc. Am. A **1**, 169–175 (1984).
41. P. V. Avizonis, F. A. Hopf, W. D. Bomberger, S. F. Jacobs, A. Tomita, and K. H. Womack, "Optical phase conjugation in a lithium formate crystal," Appl. Phys. Lett. **31**, 435–437 (1977).
42. L. Lefort and A. Barthelemy, "Revisiting optical phase conjugation by difference-frequency generation," Opt. Lett. **21**, 848–850 (1996).
43. A. Bledowski, W. Krolikowski, and A. Kujawski, "Forward

phase-conjugate wave in four-wave mixing in photorefractive media," Opt. Commun. **61**, 71–74 (1987).
44. S. H. Tang, X. H. He, and H.-Y. Zhang, "Experimental study of the forward phase-conjugate wave in degenerate four-wave mixing in $LiNbO_3$:Fe ," J. Eur. Opt. Soc. Part B **3**, 179–183 (1991).
45. F. Wang, L. Liu, and G. Li, "Self-pumped forward and backward phase conjugator with Cu-doped KNSBN crystal: caused by scattering-oscillation-amplification," Quantum Opt. **134**, 195–198 (1997).
46. A. Yariv, *Quantum Electronics* (Wiley, 1989).
47. M. Saito, A. Okamoto, K. Sato, and Y. Takayama, "Phase matching property of cross polarization four wave mixing in $BaTiO_3$ crystal," Opt. Rev. **4**, 686–690 (1997).
48. M. Zgonik, K. Nakagawa, and P. Günter, "Electro-optic and dielectric properties of photorefractive $BaTiO_3$ and $KNbO_3$," J. Opt. Soc. Am. B **12**, 1416–1421 (1995).
49. M. Zgonik, P. Bernasconi, M. Duelli, R. Schlesser, P. Günter, M. H. Garrett, D. Rytz, Y. Zhu, and X. Wu, "Dielectric, elastic, piezoelectric, electro-optic, and elasto-optic tensors of $BaTiO_3$ crystals," Phys. Rev. B **50**, 5941–5949 (1994).
50. S.-C. D. L. Cruz, S. MacCormack, J. Feinberg, Q. B. He, H.-K. Liu, and P. Yeh, "Effect of beam coherence on mutually pumped phase conjugators," J. Opt. Soc. Am. B **12**, 1363–1369 (1995).
51. N. Kukhtarev, V. B. Markov, S. G. Odulov, M. S. Soskinand, and V. L. Vinetskii, "Holographic storage ion electro-optic crystals. I. Steady-state," Ferroelectrics **22**, 949–960 (1979).